OPEN

Light: Science & Applications (2014) 3, e131; doi:10.1038/lsa.2014.12

www.nature.com/lsa

ORIGINAL ARTICLE

Spiral attractor created by vector solitons

Sergey V Sergeyev, Chengbo Mou, Elena G Turitsyna, Alexey Rozhin, Sergei K Turitsyn and Keith Blow

Mode-locked lasers emitting a train of femtosecond pulses called dissipative solitons are an enabling technology for metrology, high-resolution spectroscopy, fibre optic communications, nano-optics and many other fields of science and applications. Recently, the vector nature of dissipative solitons has been exploited to demonstrate mode locked lasing with both locked and rapidly evolving states of polarisation. Here, for an erbium-doped fibre laser mode locked with carbon nanotubes, we demonstrate the first experimental and theoretical evidence of a new class of slowly evolving vector solitons characterized by a double-scroll chaotic polarisation attractor substantially different from Lorenz, Rössler and Ikeda strange attractors. The underlying physics comprises a long time scale coherent coupling of two polarisation modes. The observed phenomena, apart from the fundamental interest, provide a base for advances in secure communications, trapping and manipulation of atoms and nanoparticles, control of magnetisation in data storage devices and many other areas.
Light: Science & Applications (2014) **3,** e131; doi:10.1038/lsa.2014.12; published online 17 January 2014

Keywords: chaos; mode-locked laser; polarisation phenomena; vector soliton

INTRODUCTION

Vector solitons (VSs) in mode-locked lasers comprise a train of stabilized short pulses (dissipative solitons[1–13]) with the specific shape defined by a complex interplay and balance between the effects of gain/loss, dispersion and nonlinearity. The state of polarisation (SOP) of the solitons either rotates with a period of a few round trips or is locked.[4–13] The stability of VSs at the different time scales from femtosecond to microseconds is an important issue to be addressed for increased resolution in metrology,[14] spectroscopy[15] and suppressed phase noise in high speed fibre optic communication.[16] In addition, there is considerable interest in achieving high flexibility in the generation and control of dynamic SOPs in the context of trapping and manipulation of atoms and nanoparticles,[17–19] control of magnetisation[20] and secure communications.[21]

The stability and evolution of VSs at a time interval from a few to thousands of cavity round trips is defined by asymptotic states (attractors) which the laser SOP approaches at a long time scale, *viz.* fixed point, periodic, quasiperiodic and chaotic dynamics. Soto-Crespo and Akhmediev[1,2] predicted theoretically based on the Ginzburg–Landau scalar model that dissipative solitons can generate strange attractors at the time scale of thousands of cavity round trips. Quantitative characterisation of strange attractors is usually based on the determination of geometric properties such as the fractal dimensionality, entropy and Lyapunov exponents.[22–26] For experimental data obtained in the form of a one-dimensional waveform (output power *vs.* time), such analysis requires the accumulation of a large amount of low noise data that is very difficult to achieve in systems where the output power is corrupted by noise. In addition, a reconstruction procedure has to be applied to obtain the attractor in the embedded three-dimensional space from the measured one-dimensional data.[22,26] High signal-to-noise ratio (>40 dB) measurement in the case of mode-locked lasers and application of a polarimeter, gives an opportunity of direct observation of attractors embedded in three-dimensional space in terms of the Stokes parameters S_1, S_2 and S_3.[12,13] Though simple forms of polarisation attractors generated by VSs, fixed points and limit cycles, have already been observed[3–13] more complex types of polarisation attractors such as chaotic ones have not yet been demonstrated.

In this article, we demonstrate the first experimental evidence of a new chaotic polarisation attractor, which results from the microsecond scale evolution of vector solitons in an erbium-doped fibre (EDF) laser mode locked with carbon nanotubes. This attractor takes the form of a double-scroll on the Poincaré sphere and has a correlation dimensionality of about 1.6. To characterize the attractor theoretically, we develop a new vector model that goes beyond the limitations of the previously used models based on either coupled nonlinear Schrödinger or Ginzburg–Landau equations.[1–11] By accounting for the vector nature of the interaction between an optical field and an active medium, the new model demonstrates that coherent coupling of two polarisation modes at a long time scale results in a double-scroll attractor with the similar correlation dimension of about 1.6 in agreement with the experiment.

MATERIALS AND METHODS

Experiment details

We use mode-locked ring cavity fibre laser the same as was studied in our previous publications[12,13] (Figure 1). As follows from our previous publications,[12] at pump current I_p=310 mA laser operates in the mode-locking regime with pulses having a fundamental soliton shape of $\mathrm{sech}^2(t/T_p)$ where T_p is a pulse width (T_p=583 fs).[12] By tuning intracavity and pump laser diode polarisation controllers, we observed

Aston Institute of Photonic Technologies, Aston University, Birmingham B4 7ET, UK
Correspondence: Dr SV Sergeyev, Aston Institute of Photonic Technologies, Aston University, Birmingham B4 7ET, UK
E-mail: s.sergeyev@aston.ac.uk
Received 19 June 2013; revised 29 August 2013; accepted 19 September 2013

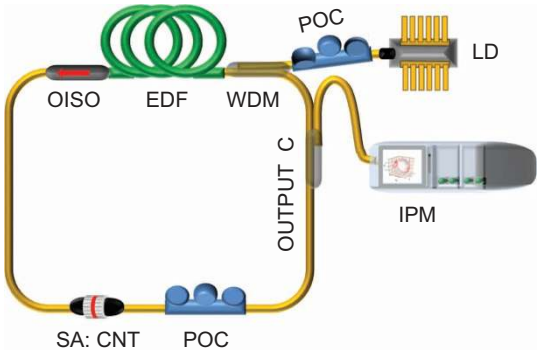

Figure 1 Experimental set-up. Laser comprises high concentration erbium-doped fibre (2 m of LIEKKITM Er80-8/125), SM fibre with anomalous dispersion, POCs, a WDM coupler, an OISO, a fast saturable absorber (polymer film with CNTs with relaxation time of 300 fs), and an output coupler. The cavity is pumped by a 976 nm LD *via* a 980/1550 WDM. Inline polarimeter (IPM5300; Thorlabs) have been used to analyse the laser output. CNT, carbon nanotube; LD, laser diode; OISO, optical isolator; POC, polarisation controller; SM, single mode; WDM, wavelength division multiplexing.

for the first time VSs slowly evolving on the surface of the Poincaré sphere on a double spiral trajectory (Figure 2a). We use polarimeter with 1 μs resolution and measurement interval of 1 ms (25–25 000 round trips) to detect normalized Stokes parameters s_1, s_2 and s_3 and the degree of polarisation (DOP). Normalized Stokes parameters and DOP are functions of the output powers of a two linearly cross-polarized SOPs $|u|^2$ and $|v|^2$and the phase difference between them $\Delta\phi$:

$$S_0=|u|^2+|v|^2,\ S_1=|u|^2-|v|^2,\ S_2=2|u||v|\cos\Delta\phi,\ S_3=2|u||v|\sin\Delta\phi,$$
$$s_i=\frac{S_i}{\sqrt{S_1^2+S_2^2+S_3^2}},\ \mathrm{DOP}=\frac{\sqrt{S_1^2+S_2^2+S_3^2}}{S_0}\ (i=1,\,2,\,3) \qquad (1)$$

The slow, as compared to the round trip, dynamics on the double spiral trajectory includes residence near the orthogonal states of polarisation for approximately 200 μs and relaxation oscillations with a period of about 8 μs (Figure 2a, 2d and 2g). In view of the residence time and oscillation period being much longer than the pulse width of 583 fs and round trip time of 38.9 ns, we have a new type of vector soliton, *viz.* polarisation precessing VS with a spiral structure quite similar to the double scroll polarisation attractors demonstrated theoretically for dye laser, vertical-cavity semiconductor laser and degenerate two-level optical medium.[27–29] The double-scroll attractor is sensitive to the external perturbations caused by small fluctuations of the lasing field due to spontaneous emission and fluctuating fibre birefringence. In the same way as for spiral chaotic attractors,[27–30] this sensitivity can lead to completely unpredictable behaviour with large variations of output dynamics (red and blue lines in Figure 2a).

By tuning the intracavity and pump laser diode polarisation controllers, we have observed a polarisation attractor in the form of a fixed point (Figure 2b). It corresponds to the conventional polarisation-locked VS with a very high degree of polarisation of 92%[12] (Figure 2e). Increasing the pump current to 330 mA and tuning the polarisation controllers, we have also found a new polarisation attractor in the form of a double semicircle (Figure 2c). In view of photodetector resolution of 1 μs, it integrates an optical signal over 25 round trips. The pulse width is of 600 fs, round trip time is of 40 ns and so amplified spontaneous emission contributes to the integrated optical signal when lasing pulse is absent. DOP for amplified spontaneous emission is close to zero and, therefore, integrated by photodetector signal will have maximum DOP <100%.

Vector model of an EDF laser model locked with carbon nanotubes

The polarisation attractors presented in the previous sections cannot be characterized in terms of coupled Schrödinger or Ginzburg–Landau equations[1–11] which are widely used to describe mode-locked lasers. The attractors have been observed in the time frame of 25–25 000 round trips. Therefore the model of the active medium has to be considered more accurately than in the typical simplified general laser models.[1–11] To address this issue, we have developed a new vector model of EDF lasers mode locked with carbon nanotubes acting as a fast saturable absorber (see Supplementary Information). The new model accounts for the dipole mechanism of the light absorption and emission in erbium and carbon nanotube (CNT), slow relaxation dynamics of erbium ions and absorption of erbium at the lasing wavelength.[27,31–33] It also includes a low-pass filter effect caused by the photodetector with a bandwidth of 1 MHz.

To simplify consideration of the dipole mechanism of the light absorption and emission in erbium and CNT, we suggest that dipole moments of the transition with absorption and emission for erbium-doped silica ($\mathbf{m}_a$,$\mathbf{m}_e$) and the dipole moment of the transition with absorption for CNT $\boldsymbol{\mu}_a$ are located in the plane defined by the orthogonal components of the lasing field $\mathbf{E}=E_x\mathbf{e}_x+E_y\mathbf{e}_y$ transverse to the direction of propagation as shown in Figure 3[32,33] (see Supplementary Information).

If we assume $\mathbf{m}_a=\mathbf{m}_e$ and use an elliptically polarized pump $\mathbf{e}_p=\left(\mathbf{e}_x+i\delta\mathbf{e}_y\right)\Big/\sqrt{1+\delta^2}$ (δ is the ellipticity of pump wave), then we obtain

$$(\mathbf{m}_e\mathbf{e}_x)=\cos\theta,(\mathbf{m}_e\mathbf{e}_y)=\sin\theta,\ \left(\mathbf{m}_a\mathbf{e}_p\right)^2=\frac{\cos^2\theta+\delta^2\sin^2\theta}{1+\delta^2}, \qquad (2)$$
$$(\boldsymbol{\mu}_a\mathbf{e}_x)=\cos\theta_1,\ (\boldsymbol{\mu}_a\mathbf{e}_y)=\sin\theta_1$$

The absorption cross-section of an elliptically polarized pump is $\sigma_{a,p}=\sigma_a^{(p)}\left(\mathbf{m}_a\mathbf{e}_p\right)^2$ and as a result, the pump light creates an orientational distribution of the population inversion $n(\theta)$[27,32,33] (Figure 3). The lasing field $\mathbf{E}=E_x\mathbf{e}_x+E_y\mathbf{e}_y$ burns a hole in this distribution with depth[27,32,33]

$$h(\theta)\sim(\mathbf{E}\mathbf{m}_e)(\mathbf{E}\mathbf{m}_e)^*=|E_x|^2\cos^2\theta+\left|E_y\right|^2\sin^2\theta+ \qquad (3)$$
$$2|E_x|\left|E_y\right|\cos(\Delta\phi)\cos\theta\sin\theta$$

As follows from Equation (3), the depth of a polarisation hole depends on the phase difference $\Delta\phi$ that results in coherent coupling of polarisation modes through gain sharing.[32,33] Note that in the scalar model the lasing field $\mathbf{E}=E_x\mathbf{e}_x+E_y\mathbf{e}_y$ burns a hole in the field distribution with depth $h\sim|E_x|^2+\left|E_y\right|^2$ and so there is no coherent coupling of the polarisation modes caused by polarisation hole burning.[1–11,27] As a result, the polarisation mode coupling is incoherent in this case, and the scalar model, which works well for the soliton description, cannot govern the observed complex dynamics. Excitation migration and upconversion in high-concentration EDFs[34–36] can result in orientation relaxation,[27] leading to transformation of the anisotropic distribution of the population inversion to isotropic. However, these processes are much slower than the time of the pulse duration and so can be neglected in the limits considered.

Numerical simulations are based on equations averaged over the short-scale dynamics for the amplitudes of the soliton pulses for two linearly polarized states of polarisation, u and v. The equations

doi:10.1038/lsa.2014.12

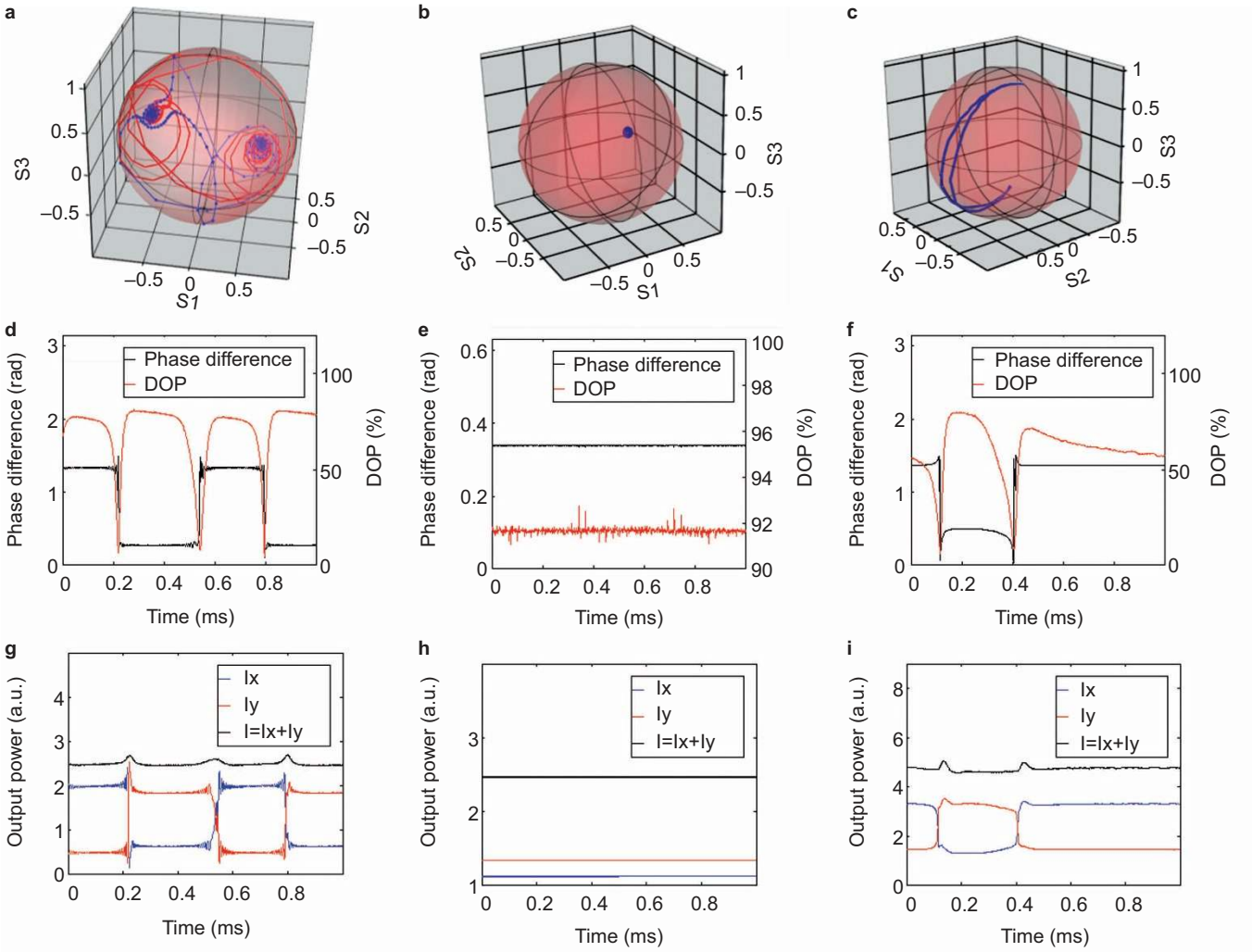

Figure 2 Experimentally obtained vector solitons in terms of (**a**–**c**) Stokes parameters at the Poincaré sphere, (**d**–**f**) phase difference and degree of polarisation and (**g**–**i**) optical power of orthogonally polarized modes I_x and I_y and total power $I=I_x+I_y$. The double-scroll attractor (blue line) is modified under external perturbations caused by small fluctuations of the lasing field due to spontaneous emission and fluctuating fibre birefringence (red line). **a**, **d**, **g** and **c**, **f**, **i**, vector solitons with the precessing state of polarisation. **b**, **e**, **h**, vector solitons with a locked state of polarisation. Parameters: time frame of 25–25 000 round trips (1 μs–1 ms). **a**, **b**, **d**, **e**, **g**, **h**, pump current I_p=310 mA. **c**, **f**, **i**, I_p=330 mA.

account for the dipole mechanism of light absorption and emission in erbium and CNT, slow dynamics of erbium ions and absorption of erbium at the lasing wavelength[27,31–33] (details of the derivation are in Supplementary Information):

$$\frac{\partial u}{\partial t_s}=i\frac{\gamma L I_{ss}}{2}\left(|u|^2u+\frac{2}{3}|v|^2u+\frac{1}{3}v^2u^*\right)+D_{xx}u+D_{xy}v,$$

$$\frac{\partial v}{\partial t_s}=i\frac{\gamma L I_{ss}}{2}\left(|v|^2v+\frac{2}{3}|u|^2v+\frac{1}{3}u^2v^*\right)+D_{xy}u+D_{yy}v,$$

$$\frac{\mathrm{d}n_0}{\mathrm{d}t_s}=\varepsilon\left[I_p+2R_{10}-\left(1+\frac{I_p}{2}+\chi R_{10}\right)n_0-\left(\chi R_{11}+\frac{I_p}{2}\frac{(1-\delta^2)}{(1+\delta^2)}\right)n_{12}-\chi n_{22}R_{12}\right],$$

$$\frac{\mathrm{d}n_{12}}{\mathrm{d}t_s}=\varepsilon\left[\frac{(1-\delta^2)}{(1+\delta^2)}\frac{I_p}{2}+R_{11}-\left(\frac{I_p}{2}+1+\chi R_{10}\right)n_{12}-\left(\frac{(1-\delta^2)}{(1+\delta^2)}\frac{I_p}{2}+\chi R_{11}\right)\frac{n_0}{2}\right],$$

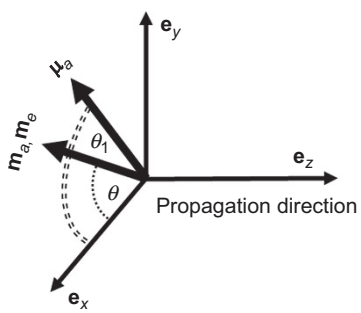

Figure 3 The orientation of dipole moments of the transition with absorption and emission for erbium-doped silica ($\mathbf{m}_a$,$\mathbf{m}_e$) and the dipole moment of the transition with absorption for CNT $\boldsymbol{\mu}_a$. CNT, carbon nanotube.

$$\frac{dn_{22}}{dt_s}=\varepsilon\left[R_{12}-\left(\frac{I_p}{2}+1+\chi R_{10}\right)n_{22}-\chi R_{12}\frac{n_0}{2}\right],$$

$$R_{10}=\frac{1}{\pi\left(1+\Delta^2\right)}\left(|u|^2+|v|^2\right),\ R_{11}=\frac{1}{\pi\left(1+\Delta^2\right)}\left(|u|^2-|v|^2\right),$$
$$R_{12}=\frac{1}{\pi\left(1+\Delta^2\right)}\left(uv^*+vu^*\right) \quad (4)$$

Coefficients D_{ij} can be found as follows:

$$D_{xx}=\frac{\alpha_1 L(1-i\Delta)}{1+\Delta^2}(f_1+f_2)-\left(\frac{\alpha_2 L}{2}-\frac{2\alpha_2\alpha_3 L}{8\pi}k_1\right)-\alpha_4 L,$$
$$D_{yy}=\frac{\alpha_1 L(1-i\Delta)}{1+\Delta^2}(f_1-f_2)-\left(\frac{\alpha_2 L}{2}-\frac{\alpha_2\alpha_3 L}{4\pi}k_2\right)-\alpha_4 L, \quad (5)$$
$$D_{xy}=D_{yx}=\frac{\alpha_1 L(1-i\Delta)}{1+\Delta^2}f_3-\frac{2\alpha_2\alpha_3 L}{8\pi}k_3$$

where

$$f_1=\left(\chi\frac{n_0}{2}-1\right),\ f_2=\chi\frac{n_{12}}{2},\ f_3=\chi\frac{n_{22}}{2},$$
$$k_1=3|u|^2+|v|^2,\ k_2=|u|^2+3|v|^2,\ k_3=uv^*+vu^* \quad (6)$$

for a vector model of EDF and CNT:

$$f_1=\left(\chi\frac{n_0}{2}-1\right),\ f_2=\chi\frac{n_{12}}{2},f_3=\chi\frac{n_{22}}{2},\ k_1=k_2=|u|^2+|v|^2,k_3=0 \quad (7)$$

for a vector model of EDF and a scalar model of CNT:

$$f_1=\left(\chi\frac{n_0}{2}-1\right),\ f_2=f_3=0,\ k_1=3|u|^2+|v|^2,$$
$$k_2=|u|^2+3|v|^2,\ k_3=uv^*+vu^* \quad (8)$$

for a scalar model of EDF and a vector model of CNT:

$$f_1=\left(\chi\frac{n_0}{2}-1\right),\ f_2=f_3=0,\ k_1=k_2=|u|^2+|v|^2,\ k_3=0 \quad (9)$$

for a scalar model of EDF and CNT.

Here $t_s=z/\left(V_g t_R\right)$ is a slow-time variable, $\varepsilon=t_R\gamma_d$, γ_d is the rate of relaxation for population inversion in EDF, $t_R=L/V_g$ is the photon round-trip time, V_g is the group velocity, L is the cavity length, $|u|^2$ and $|v|^2$ are normalized to the saturation power I_{ss}, the pump power I_p is normalized to the saturation power I_{ps} ($I_{ps}=\gamma_d A/\left(\sigma_a^{(p)}\Gamma_p\right)$, $I_{ss}=\gamma_d A/\left(\sigma_a^{(L)}\Gamma_L\right)$), Γ_L and Γ_p are the confinement factors of the EDF at the lasing and pump wavelengths, $\sigma_{a(e)}^{(L)}$ and $\sigma_a^{(p)}$ are absorption and emission cross-sections at the lasing wavelength λ_L and at the pump wavelength λ_p, A is the fibre core cross-section area, δ is the ellipticity of the pump wave, Δ is the detuning of the lasing wavelength with respect to the maximum of the gain spectrum, $\alpha_1=\sigma_a\Gamma_L\rho$ and α_2 are EDF and CNT absorption coefficients at the lasing wavelength, ρ is the concentration of erbium ions, $\chi=\left(\sigma_a^{(L)}+\sigma_e^{(L)}\right)/\sigma_a^{(L)}$, α_3 is the ratio of saturation powers for CNT and EDF, α_4 is the linear loss coefficient, the Kerr coupling constant is $\gamma=2\pi n_2/(\lambda_L A)$, where n_2 is the nonlinear Kerr coefficient and A_{eff} is the effective core area of the fibre.

We consider the case when the intracavity polarisation controller compensates the phase and amplitude anisotropy caused by any fibre birefringence and polarisation-dependent losses. The angular distribution of erbium ions at the first excited level $n(\theta)$ can be expanded into a Fourier series as follows:[32,33]

$$n(\theta)=\frac{n_0}{2}+\sum_{k=1}^{\infty}n_{1k}\cos(k\theta)+\sum_{k=1}^{\infty}n_{2k}\sin(k\theta) \quad (10)$$

In the experiment, a fibre patchcord of 5 m has been placed between the output of the laser and the polarimeter. We account for SOP distortions caused by the patchcord as the composition of POC and a birefringent element placed at the output of the laser:[37]

$$\begin{bmatrix}u_{pol}\\ v_{pol}\end{bmatrix}=\begin{bmatrix}A+iB & C+iD\\ -C+iD & A-iB\end{bmatrix}$$
$$\begin{bmatrix}\exp(i2\pi L/L_b) & 0\\ 0 & \exp(-i2\pi L/L_b)\end{bmatrix}\begin{bmatrix}u_L\\ v_L\end{bmatrix},$$

$$A=-\cos\psi_1\cos\psi_2,\ B=-\sin\psi_3\sin\psi_1,$$
$$C=-\cos\psi_1\sin\psi_2,\ D=-\sin\psi_1\cos\psi_3,$$
$$\psi_1=\gamma-\alpha-\xi/2,\ \psi_2=\xi/2, \quad (11)$$
$$\psi_3=\xi/2+\alpha,\ A^2+B^2+C^2+D^2=1$$

Here $u_{L(pol)}$ and $v_{L(pol)}$ are the electric field components at the output of the laser and at the input of the polarimeter; $\alpha/2$, $\gamma/2$ and $(\alpha+\xi)/2$ are the orientation of the first quarter wave plate, half wave plate and the second quarter wave plate with respect to vertical axis, L_b is a birefringence beat length. We have used parameters which are quite close to the experimental ones, *viz.* $L=10$ m, $\alpha_1 L=200/\ln 10$, $\alpha_2 L=0.136$, $\alpha_3=10^{-4}$, $\alpha_4 L=50/\ln 10$, $\chi=5/3$, $\Delta=0.1$, $I_p=30$, $\gamma L I_{ss}=2\times10^{-6}$, $\varepsilon=10^{-4}$, $L/L_c=1.05$, $A=0.05$, $B=0.2$ and $C=0.05$.

We have applied two-level model instead of three- and four-level models[34–36,38,39] that is justified for EDFs in view of populations of the first n, second n_2 and third n_3 excited levels are related as follows $n>>n_2>>n_3$.[38,39] We also neglected excited state absorption (ESA) in Equation (4) that is justified if inequality $I_p(\sigma_{\text{ESA}}+\sigma_a^{(p)})/I_{ps}\sigma_a^{(p)}<<\gamma_d\tau_2$ holds.[35] Here σ_{ESA} is excited state absorption cross-section and τ_2 is the second excited level lifetime. Specifications of high-concentration EDF Er8-8/125 are the following: $\sigma_{\text{ESA}}<\sigma_a^{(p)}$,[39] $\tau_2=10$ μs, $\gamma_d=100\ \text{s}^{-1}$, $\rho=6.3\times10^{25}$ ions m^{-3}, and mode filed diameter $d=9.5$ μm. As follows from these data and notations to Equations (4)–(9), $I_{ps}\sim4.4$ mW and $\gamma_d\tau_2=10^3$ and so for $I_p=170$ mW used in experiments aforementioned inequality holds. We have also neglected the dynamics of the absorption in CNT that holds when saturable absorber relaxation τ_a time is smaller than the pulse width T_p. In our experiments, $\tau_a\sim300$ fs and $T_p\sim600$ fs and so approximation of fast saturable absorber will be still valid if we make change of variables $\alpha_2\rightarrow\alpha_2(1-\exp(-T_p/\tau_a))$ for the case of $\alpha_2<<1$. Though ansatz (7) in Supplementary Information can be used only if the pulse width of the fundamental solion is fixed that is confirmed by our experimental study, ansatz which separates fast and slow time variables can be used for different pulse shapes with fixed pulse widths (for example, Gaussian in the case of normal dispersion). If states of polarisation for adjacent pulses in multipulse or in bound state soliton regimes are the same and phase shift and pulse separation for bound state are fixed, Equations (4)–(9) can be still valid to describe SOP evolution for such multipulse and bound state regimes. To describe SOP evolution for the soliton regimes with evolving pulse parameters, the more general equation (6) in Supplementary Information can be used after minor revisions to account for gain spectral bandwidth and cavity anisotropy caused by in-cavity polarisation controller.

doi:10.1038/lsa.2014.12

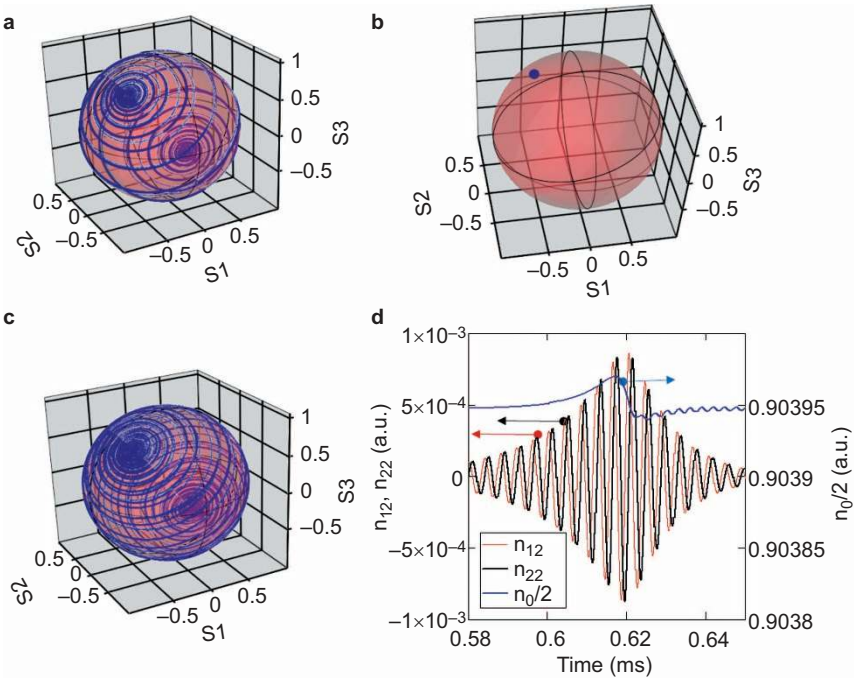

Figure 4 Theoretically obtained: (**a**, **c**) polarisation precessing and (**b**) polarisation-locked vector solitons in terms of (**a**–**c**) Stokes parameters at the Poincaré sphere and (**d**) dynamics of the components n_0, n_{12} and n_{22} of the orientational distribution of inversion $n(\theta,t)=\frac{n_0(t)}{2}+n_{12}(t)\cos(2\theta)+n_{22}(t)\sin(2\theta)$ corresponding to the case **a**. Parameters (details are in the section on 'materials and methods'): **a**–**c**, $\varepsilon=10^{-4}$, $\alpha_1 L=200/\ln 10$, $\alpha_2 L=0.136$, $\alpha_3=10^{-4}$, $\alpha_4 L=50/\ln 10$, $\chi=5/3$, $\Delta=0.1$, $\gamma L I_{ss}=2\times10^{-6}$; **a**, $I_p=30$, $\delta=1$; **b**, $I_p=30$, $\delta=0.8$; **c**, $I_p=100$, $\delta=0.99$.

Sergeyev *et al.*[34–36] have shown that migration assisted upconversion in high-concentration EDF results in decreasing first excited lifetime more than 10 times and in change of pump power distribution and so gain distribution along the fibre.[34] Model based on Equations (4)–(9) is discrete rather than distributed one and so we are able to mimic effect of upconversion accelerated by migration by decreasing the lifetime only.

RESULTS AND DISCUSSION

Numerical simulations using the developed vector model are shown in Figure 4. All the results in Figure 4 correspond to the case when the polarisation controller compensates all anisotropy in the cavity and only an external fibre patchcord transforms the output lasing SOP. Anisotropy in the cavity is caused by the elliptically polarized pump. Figure 4 shows that a double-scroll attractor appears if laser cavity is symmetrical, i.e., when the pump is circularly polarized, with ellipticity $\delta=1$ (Figure 4a). When the pump SOP becomes more elliptical with $\delta=0.8$ and the system becomes more anisotropic, the system approaches the steady state solution (Figure 4b). Increased pump and weak deviation of the pump SOP from the circular to the elliptical ($\delta=0.99$) distorts the symmetry and the trajectories fill more densely the surface of the Poincaré sphere (Figure 4c). The orientation distribution of the inversion can be written as Equation (10) where, according to Equation (3), $n_{22}(t)\sim\cos\Delta\phi(t)$. As follows from Figure 4d, $n_{22}(t)\neq0$ and so polarisation hole burning with a depth proportional to $n_{22}(t)$ results in coherent coupling of the polarisation modes and, therefore, in the complex behaviour shown in Figure 4a.

We have found that the low-pass filter effect of a photodetector with cutoff frequency of 1 MHz can affect the appearance of the attractors in Figure 4. By using a low-pass filter with a Hanning window (transmission spectrum $T(f)=(1+\cos(\pi f/f_c))/2$, $f\leq f_c=1$ MHz), we have processed the time domain waveforms shown in Figure 4. As a result of the low-pass filter effect, the double-scroll attractor in Figure 4a is slightly modified showing remarkable similarity to the attractor observed experimentally (Figures 2a, 5a, 5d and 5g). Note that such filtering does not affect a polarization-locked attractor (Figure 5b, 5e and 5h). However, the low-pass filter transforms the fast trajectory rotation on the Poincaré sphere shown in Figure 4c to the slow evolution on the double semicircle trajectory similar to the experimentally observed one (Figures 2c, 2f , 2i, 5c, 5f and 5i). Presented in Figures 2a, 2d, 2g, 5a, 5d and 5g, spiral attractor comprises dynamics related to the relaxation oscillations. Period of the oscillations can be estimated in terms of round trip time and notations to Equation (4) as $T_{osc}\sim\varepsilon^{1/2}$.[40] With 40 ns round trip time and $\varepsilon=10^{-4}$, we have $T_{osc}\sim4$ μs. If gain dynamics is neglected, then $\varepsilon\to\infty$ in Equation (4) and so $T_{osc}\to\infty$ that means the absence of auto-oscillations and, therefore, spiral attractor cannot be found. Thus, Equation (4) cannot be further simplified and slow gain dynamics has to be accounted for.

The results can be interpreted in terms of coupled oscillators' theory where weak coupling leads to a complex behaviour, while increase in the coupling strength leads to the oscillation quenching and appearance of the globally stable steady state (the Bar–Eli effect[41]). Thus, the coupling in our system is determined by the pump SOP and power. In addition to this, orthogonally polarized laser modes are coupled through gain sharing, detuning of the lasing wavelength with respect to the maximum of the gain spectrum and the self-phase modulation caused by the Kerr nonlinearity.

To find the contribution of each of these factors to the origin of the spiral attractor, we have investigated three distinct cases: (i) scalar model of the erbium-active medium, and a vector model of CNT; (ii) a scalar model of both erbium-active medium and CNT; and (iii) a vector model of the active erbium medium, and a scalar model of

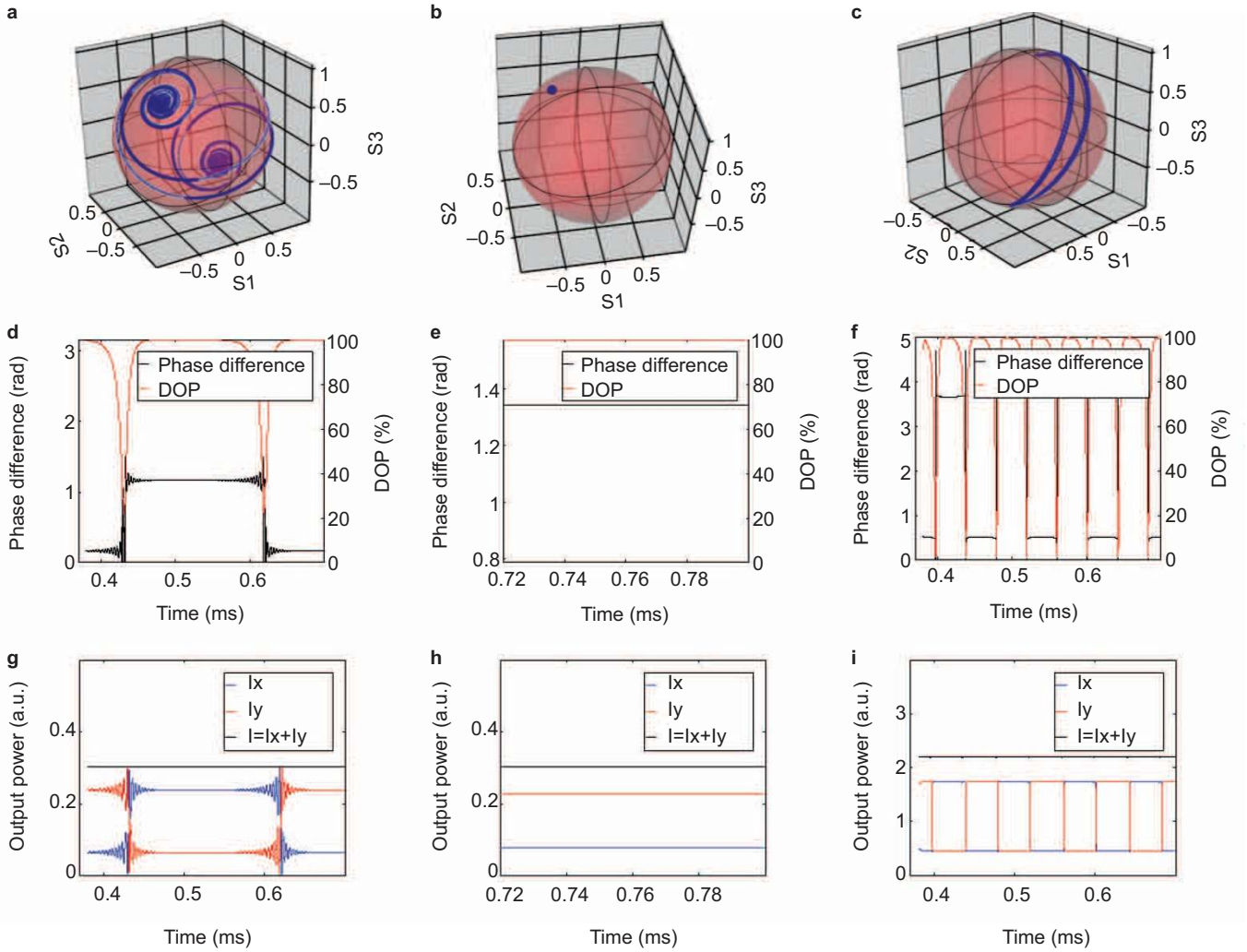

Figure 5 Numerical simulation results. (**a**–**c**) Spiral attractor. (**d**–**f**) Transformation of the double-scroll attractor to the double semi-circle by data filtering. (**g**) Low-pass filter with a Hanning window (transmission spectrum $T(f)=(1+\cos(\pi f/f_c))/2, f\le f_c=1$ MHz). (**h**, **i**) Polarisation-locked vector soliton. Parameters: **a**–**f**, **h**–**i**, $\varepsilon=10^{-4}$, $\alpha_1 L=200/\ln 10$, $\alpha_2 L=0.136$, $\alpha_3=10^{-4}$, $\alpha_4 L=50/\ln 10$, $\chi=5/3$, $\Delta=0.1$, $\gamma L I_{ss}=2\times10^{-6}$; **a**–**c**, $I_p=30$, $\delta=1$; **d**–**f**, $I_p=100$, $\delta=0.99$; **h**, **i**, $I_p=30$, $\delta=0.8$.

CNT at $\Delta=0$ (Δ is detuning of the lasing wavelength with respect to the maximum of the gain spectrum). First, we linearized the equations by substituting $|u|=|u_0|+x_1$, $|v|=|v_0|+x_1$,$\Delta\phi=\Delta\phi_0+x_3$, $f_1=f_{10}+x_4$, $f_2=f_{20}+x_5$, $f_3=f_{30}+x_5$ and account for the different coefficients for the cases i– iii. Here $|u_0|$, $|v_0|$, $\Delta\phi_0$, f_{10}, f_{20} and f_{30} are steady-state solutions for the cases i–iii:

$$|u_0|^2=|v_0|^2=\frac{\pi\alpha_1}{2\chi\alpha_4}\left(\frac{I_p}{2}(\chi-1)-1\right)-\frac{\pi(1+\Delta^2)}{2\chi}\left(1+\frac{I_p}{2}\right),$$
$$\Delta\phi_0=\pm\frac{\pi}{2},\ f_{10}=\frac{I_p(\chi-1)/2-1}{1+I_p/2+2\chi|u_0|^2/(1+\Delta^2)\pi},\ f_{20}=f_{30}=0 \quad (12)$$

where $u=|u|\exp(\phi_u)$, $v=|v|\exp(\phi_v)$ and $\Delta\phi=\phi_u-\phi_v$ is the phase difference between two linearly polarized states of polarisation. The equations are valid for $\alpha_3(|u|^2+|v|^2)/\pi<<1$. Substituting $x_i=\tilde{x}_i\exp(\lambda t_s)$ into the linearized equations, we find the following eigenvalues:

$$\lambda_{1,2}=\pm2\sqrt{a_1^2+a_2^2},$$
$$\lambda_{3,4}=\frac{-b_2+4a_1}{2}\pm\frac{1}{2}\sqrt{(b_2+4a_1)^2-8a_3b_1} \quad \text{(case i)}$$

$$\lambda_1=2a_2,\ \lambda_2=-2a_2,$$
$$\lambda_{3,4}=\frac{-b_2+4a_1}{2}\pm\frac{1}{2}\sqrt{(b_2+4a_1)^2-8a_3b_1} \quad \text{(case ii)}$$

$$\lambda_{1,2}=\frac{-b_2+2a_1}{2}\pm\frac{1}{2}\sqrt{(b_2+2a_1)^2-4a_3b_1},$$
$$\lambda_{3,4}=\frac{-b_2-4a_1}{2}\pm\frac{1}{2}\sqrt{(b_2-4a_1)^2-8a_3b_1}, \quad \text{(case iii)} \ (13)$$
$$\lambda_{5,6}=\frac{-b_2+4a_1}{2}\pm\frac{1}{2}\sqrt{(b_2+4a_1)^2-8a_3b_1}$$

doi:10.1038/lsa.2014.12

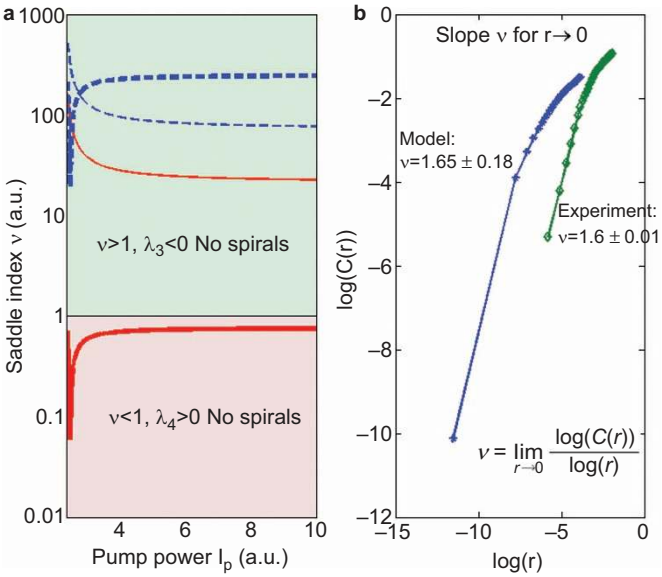

Figure 6 (**a**) Saddle index ν as a function of the normalized pump power I_p for the first case (solid line) and the second case (dashed line). Parameters (thin and thick lines): $\varepsilon=10^{-4}$, $\alpha_1 L=200/\ln 10$, $\alpha_2 L=0.136$, $\alpha_4 L=50/\ln 10$, $\chi=5/3$, $\Delta=0.1$, $\delta=1$, $\gamma L I_{ss}=2\times10^{-6}$; (thin lines): $\alpha_3=10^{-4}$; (thick lines): $\alpha_3=10^{-2}$. (**b**) Correlation function *vs.* the distance between points on the Poincaré sphere.

where

$$a_1=\frac{\alpha_2 L\alpha_3|u_0|^2}{2\pi},a_2=\frac{2\gamma L I_{ss}|u_0|^2}{3},a_3=\frac{\alpha_1 L}{1+\Delta^2},$$
$$b_1=\varepsilon\chi f_{10}\frac{2|u_0|^2}{(1+\Delta^2)\pi},b_2=\varepsilon\left(1+\frac{I_p}{2}+\frac{2\chi|u_0|^2}{(1+\Delta^2)\pi}\right) \quad (14)$$

Next, we have introduced a saddle index as follows[30]

$$\nu=|\rho/\gamma|,\ \text{If}\ \lambda_1=\gamma>0,\ \lambda_{2,3}=-\rho\pm i\omega,\ (\omega\neq0,\rho>0),$$
$$\text{or}\ \lambda_1=-\gamma<0,\ \lambda_{2,3}=\rho\pm i\omega\ (\omega\neq0,\rho>0) \quad (15)$$

Equation (15) describes saddle focus where limit cycles can emerge in the homoclinic bifurcation. According to the Shilnikov theorem, the stability and number of the limit cycles depends on the saddle index ν.[30] If $\nu>1$, homoclinic bifurcations results in one stable limit cycle. Unlike this, for $\nu<1$, an infinite number of unstable cycles can emerge and form a chaotic attractor.[30] The saddle index as a function of pump power I_p is shown in Figure 6a. As follows from Figure 6a, the double-scroll attractor cannot exist for the first and the second case. For the third case, we have obtained eigenvalues $\lambda_i=-\rho_i\pm i\omega_i$ ($\omega_i\neq0$, $\rho_i>0$) and so the double-scroll attractor cannot exist as well. Thus, the detuning of the lasing wavelength with respect to the maximum of the gain spectrum along with the coherent mode coupling through the gain sharing must have lead to the complex dynamics.

The attractors shown in Figures 2 and 5 are different from the classical double-scroll strange Lorenz attractor obtained for single mode lasers.[40,42] The Lorenz attractor is embedded in three-dimensional space, while the attractors in Figures 2 and 4 are located on the surface of the Poincaré sphere, i.e., are embedded in two-dimensional space. Strange attractors are typically characterized by fractal dimensionality d, which is smaller than the dimensionality of the space in which the attractors are embedded.[24,25] Herein we applied the Grassberger–Procaccia algorithm for the calculation of the correlation dimension ν, which is related to the dimension d as $\nu\leqslant d$.[24,25] This measure is obtained based on a consideration of correlation between points of the time series on the attractor, i.e., for our case, $\{x_{kj}\}$, $k=0, 1, \ldots, N$; $j=0, 1, \ldots, N$ (N is the number of points), where

$$x_{kj}=\arccos\left(s_{1,k}s_{1,j}+s_{2,k}s_{2,j}+s_{3,k}s_{3,j}\right),$$
$$C(r)=\frac{1}{N^2}\sum_{k=0}^{N}\sum_{j=0}^{N}\theta\left(r-|x_{kj}|\right), \quad (16)$$
$$\theta\left(r-|x_{kj}|\right)=\begin{vmatrix}1\ \text{if}\ |x_{kj}|\leq r\\ 0\ \text{if}\ |x_{kj}|>r\end{vmatrix},\ r=[0,\pi]$$

As a result, the correlation dimension ν can then be found as follows:[24,25]

$$\nu=\lim_{r\to0}\frac{\log(C(r))}{\log(r)} \quad (17)$$

The results are shown in Figure 6b. We found that $\nu\sim1.6$ for the double-scroll attractors in Figures 2a and 4b. Thus, the dimension obtained indicates that the observed double-scroll attractor could be a new strange attractor.

CONCLUSIONS

In summary, we demonstrate experimentally and theoretically a novel type of VS in EDF lasers mode locked with carbon nanotubes. Slow polarisation dynamics of this soliton measured in the time frame of 25–25 000 round trips takes the shape of a double-scroll chaotic attractor on the Poincaré sphere. Applying the Grassberger–Procaccia algorithm, we calculated a correlation dimension of 1.6 that is evidence of a new strange attractor in addition to only a few already experimentally observed in laser physics, *viz.* Lorenz, Rössler and Ikeda strange attractors.[22–26,40,42] The descriptions of new structures are found to be beyond the standard models of mode-locked lasers based on coupled Schrödinger or Ginzburg–Landau equations. Therefore, we have developed a new model accounting for the dipole mechanism of the light absorption and emission in erbium and CNT, slow relaxation dynamics of erbium ions and absorption of erbium at the lasing wavelength. As a result, a new chaotic attractor has been reproduced theoretically for parameters close to the experimental ones. By unveiling the origin of new types of unique states of polarisation evolving on very complex trajectories, our theoretical and experimental studies pave the way to new techniques in metrology,[14] high-resolution femtosecond spectroscopy,[15] high-speed and secure fibre optic communications,[16,21] nano-optics (trapping and manipulation of nanoparticle and atoms[17–19]) and spintronics (vector control of magnetisation[20]). With further advances in the development of fast polarimetry in the context of speed (>1 GHz) and the number of stored samples (>10 M samples), the mode-locked laser with polarisation controller will become a demonstrator of the complex dynamics including dynamic chaos like a generic Chua circuit.[23] It will open the possibility for creating fundamentally new types of lasers with controlled dynamical states of polarisation.

ACKNOWLEDGMENTS

Support of the ERC, EPSRC (project UNLOC, EP/J017582/1) and FP7-PEOPLE-2012-IAPP (project GRIFFON, No. 324391) is acknowledged.

1 Grelu P, Akhmediev N. Dissipative solitons for mode-locked lasers. *Nat Photon* 2012; **6**: 84–92.
2 Soto-Crespo JM, Akhmediev N. Soliton as strange attractor: nonlinear synchronization and chaos. *Phys Rev Lett* 2005; **95**: 024101.

3 Haus JW, Shaulov G, Kuzin EA, Sanchez-Mondragon J. Vector soliton fiber lasers. *Opt Lett* 1999; **24**: 376–378.
4 Cundiff ST, Collings BC, Akhmediev NN, Soto-Crespo JM, Bergman K *et al*. Observation of polarization-locked vector solitons in an optical fiber. *Phys Rev Lett* 1999; **82**: 3988–3991.
5 Collings BC, Cundiff ST, Akhmediev NN, Soto-Crespo JM, Bergman K *et al*. Polarization-locked temporal vector solitons in a fiber laser: experiment. *J Opt Soc Am B* 2000; **17**: 354–365.
6 Barad Y, Silberberg Y. Polarization evolution and polarization instability of solitons in birefringent optical fibers. *Phys Rev Lett* 1997; **78**: 3290–3293.
7 Silberberg Y, Barad Y. Rotating vector solitary waves in isotropic fibers. *Opt Lett* 1995; **20**: 246–248.
8 Zhang H, Tang DY, Zhao LM, Tam HY. Induced solitons formed by cross polarization coupling in a birefringent cavity fiber laser. *Opt Lett* 2008; **33**: 2317–2319.
9 Zhao LM, Tang DY, Zhang H, Wu X. Polarization rotation locking of vector solitons in a fiber ring laser. *Opt Express* 2008; **16**: 10053–10058.
10 Zhang H, Tang DY, Zhao LM, Wu X. Observation of polarization domain wall solitons in weakly birefringent cavity fiber lasers. *Phys Rev E* 2009; **80**: 052302.
11 Tang DY, Zhang H, Zhao LM, Wu X. Observation of high-order polarization-locked vector solitons in a fiber laser. *Phys Rev Lett* 2008; **101**: 153904.
12 Mou Ch, Sergeyev SV, Rozhin A, Turitsyn SK. All-fiber polarization locked vector soliton laser using carbon nanotubes. *Opt Lett* 2011; **36**: 3831–3833.
13 Sergeyev SV, Mou Ch, Rozhin A, Turitsyn SK. Vector solitons with locked and precessing states of polarization. *Opt Express* 2012; **20**: 27434–27440.
14 Udem Th, Holzwarth R, Hänsch TW. Optical frequency metrology. *Nature* 2002; **416**: 233–237.
15 Mandon J, Guelachvili G, Picqué N. Fourier transform spectroscopy with a laser frequency comb. *Nat Photon* 2009; **3**: 99–102.
16 Hillerkuss D, Schmogrow R, Schellinger T, Jordan M, Winter M *et al*. 26 Tbit s^{-1} 21 line-rate super-channel transmission utilizing all-optical fast Fourier transform processing. *Nat Photon* 2011; **5**: 364–371.
17 Jiang Y, Narushima T, Okamoto H. Nonlinear optical effects in trapping nanoparticles with femtosecond pulses. *Nat Phys* 2010; **6**: 1005–1009.
18 Tong L, Miljković VD, Käll M. Alignment, rotation, and spinning of single plasmonic nanoparticles and nanowires using polarization dependent optical forces. *Nano Lett* 2010; **10**: 268–273.
19 Spanner M, Davitt KM, Ivanova MY. Stability of angular confinement and rotational acceleration of a diatomic molecule in an optical centrifuge. *J Chem Phys* 2001; **115**: 8403–8410.
20 Kanda N, Higuchi T, Shimizu H, Konishi K, Yoshioka K *et al*. The vectorial control of magnetization by light. *Nat Commun* 2011; **2**: 362.
21 van Wiggeren GD, Roy R. Communication with dynamically fluctuating states of light polarization. *Phys Rev Lett* 2002; **88**: 097903.
22 Schuster HG, Just W. *Deterministic Chaos. An Introduction*. Weinheim: Wiley-VCH Verlag GmbH & Co. KGaA; 2005.
23 Chua LO, Pivka L, Wu CW. A universal circuit for studying chaotic phenomena. *Philos Trans R Soc Lond A Phys Sci Eng* 1995; **353**: 65–84.
24 Grassberger P, Procaccia I. Characterization of strange attractors. *Phys Rev Lett* 1983; **50**: 346–349.
25 Lukashchuk S, Fal'kovich G, Chernykh A. Calculation of the dimensions of attractors from experimental data. *J Appl Mech Tech Phys* 1989; **30**: 95–100.
26 Virte M, Panajotov K, Thienpont H, Sciamanna M. Deterministic polarization chaos from a laser diode. *Nat Photon* 2013; **7**: 60–65.
27 Sergeyev SV. Spontaneous light polarization symmetry breaking for an anisotropic ring cavity dye laser. *Phys Rev A* 1999; **59**: 3909–3917.
28 Byrne JA, Gabitov IR, Kovačič G. Polarization switching of light interacting with a degenerate two-level optical medium. *Physica D* 2003; **186**: 69–92.
29 Willemsen MB, van Exter MP, Woerdman JP. Polarization loxodrome of a vertical-cavity semiconductor laser. *Opt Commun* 2001; **199**: 167–173.
30 Ovsyannikov IM, Shilnikov LP. On systems with a saddle-focus homoclinic curve. *Math USSR Sb* 1987; **58**: 557–574.
31 Saleh AA, Jopson RM, Evankow JD, Aspell J. Modeling of gain in erbium-doped fiber amplifiers. *IEEE Photon Technol Lett* 1990; **2**: 714–717.
32 Zeghlache H, Boulnois A. Polarization instability in lasers. I. Model and steady states of neodymium-doped fiber lasers. *Phys Rev A* 1995; **52**: 4229–4242.
33 Leners R, Stéphan G. Rate equation analysis of a multimode bipolarization Nd^{3+} doped fibre laser. *Quantum Semiclass Opt* 1995; **7**: 757–794.
34 Sergeyev S. Model of high-concentration erbium-doped fibre amplifier: effects of migration and upconversion processes. *Electron Lett* 2003; **39**: 511–512.
35 Sergeyev SV, Popov S, Khoptyar D, Friberg AT, Flavin D. Statistical model of migration-assisted upconversion processes in high-concentration erbium-doped fiber amplifier. *J Opt Soc Am B* 2006; **23**: 1540–1543.
36 Sergeyev SV, Popov S, Friberg AT. Influence of short-range coordination order on excitation migration and upconversion in multicomponent glasses. *Opt Lett* 2005; **30**: 1258–1260.
37 Heismann F. Analysis of a reset-free polarization controller for fast automatic polarization stabilization in fiber-optic transmission systems. *J Lightwave Technol* 1994; **12**: 690–699.
38 Roldán E, de Valcárcel GJ, Mitschke F. Role of field losses on the Risken–Nummedal–Graham–Haken laser instability: application to erbium-doped fibre lasers. *Appl Phys B* 2003; **76**: 741–748
39 Desurvire E. *Erbium-Doped Fiber Amplifiers, Principles and Applications*. New York: John Wiley & Sons; 1994.
40 Khanin YA. *Fundamentals of Laser Dynamics*. Cambridge: Cambridge International Science Publishing; 2005.
41 Aronson DG, Ermentrout GB, Kopell N. Amplitude response of coupled oscillators. *Physica D* 1990; **41**: 403–449.
42 van Tartwijk GH, Agrawal GP. Laser instabilities: a modern perspective. *Prog Quant Electron* 1998; **22**: 43–122.

Supplementary Information for this article can be found on *Light: Science & Applications*' website (http://www.nature.com/lsa/).